Chapter 4

Mathematical Analysis of Electrical Breakdown Effects in Waveguides

Isaac Medina and Primo-Alberto Calva

Additional information is available at the end of the chapter

http://dx.doi.org/10.5772/intechopen.76973

Abstract

The designers of microwave devices in the industry use the analytical solutions of the corona discharge equation to determine the minimum power breakdown threshold, in a particular device, such as waveguides and filters, and know whether it is in the established margins. There are two main ways to determine the breakdown threshold of a waveguide analytically; the most commonly used describes the plasma density generation completely as a function of the geometry by using the characteristic diffusion length, while the second is a more thorough method that involves the use of the effective diffusion length which considers collision frequency and electric field into the equations. Hence the aim of the designers is to obtain the closest results to experimental results, both methods must be considered in addition to the environmental changes so that they know the operational limits. This chapter describes the different methods to obtain analytical results for the breakdown threshold in any rectangular waveguide device, the influence of environmental conditions in the analysis and the inhomogeneous electric field effect inside the devices.

Keywords: electrical breakdown threshold, corona, characteristic diffusion length, waveguide filters, effective diffusion length

1. Introduction

Traffic capacity in a high-frequency scenario where waveguides are involved is generally limited by two main factors: bandwidth and input power [1]. In cases where the atmospheric pressure is a factor, such as satellite communications, the maximum input power of the signal is determined by several factors, among which are the geometry of the device, the collision

frequency of the molecules and free electrons and the intrinsic characteristics of the propagating medium itself, that is, air or nitrogen [2].

Waveguides are conductor hollow tubes, generally consisting of a circular, elliptical, or rectangular cross-section. The cross-section dimensions are chosen by designers in such a way that electromagnetic waves propagate inside the guide. A waveguide can have several shapes and sizes, and frequently its performance is a function of the radiofrequency (RF) routing signals; this means that the way the wave is propagating inside the guide. Rectangular waveguides are the most commonly used; this is because they are easily fabricated, they have a very broad bandwidth and they present low losses within their operating frequencies [3].

Rectangular waveguides operate only in certain frequency bands, depending on the cross-section dimensions. Waveguide geometry determines the highest operating wavelength, this means, higher waveguide sizes operate at lower frequencies.

Waveguide filters are responsible of eliminating unwanted radiations and interferences in a communication scheme. These devices are also hollow conductor tubes, made generally of aluminium, with the difference that inside them are distance variations or obstructions that generate the wanted filtering effect. **Figure 1** shows different types of waveguide filters.

The reason waveguide filters are analysed in terms of breakdown power is because this device is with the shortest cross-section of all the communications system, reaching even distances of 1 mm. In these sections, electric field density can be so high that it leads to electrical breakdown, rendering the components useless. **Figure 2** shows a low-pass corrugated filter after breakdown has occurred [4].

The continuous miniaturization tendency in electronic devices and the increasing demand of services lead to higher component integration. In a transponder system, passive components are allocated, such as filters and waveguides, where, due to the used power, high densities of electric field are reached, presenting mainly the corona and multipactor effects [5].

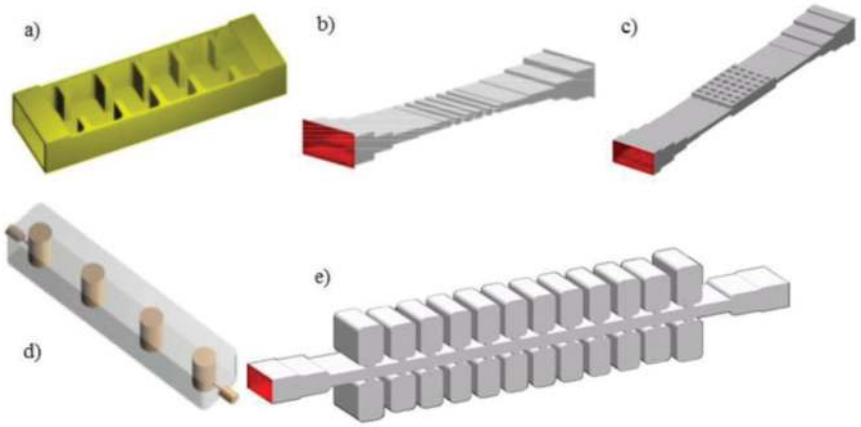

Figure 1. (a) Coupled iris filter, (b) corrugated waveguide filter, (c) waffle iron filter, (d) posts filter, and (e) guarded waveguide filter.

http://dx.doi.org/10.5772/intechopen.76973

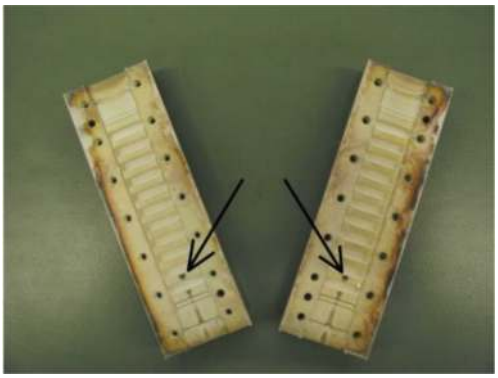

Figure 2. Low-pass corrugated filter after breakdown has occurred, as reported in [4].

High-performance RF filters are widely used in communications systems, where it is necessary to know its capabilities for input power handling. Since increasing the power levels is the simpler way to impulse the reach of the system and its capability for data transmission, the design for the high-power operation filters must consider the next effects: electrical breakdown by ionization (corona effect), multipactor effect and passive intermodulation interferences (PIM).

Multipactor is a breakdown mechanism in vacuum, in which a resonant increase of free-electron space charge develops between two surfaces. The applied field intensity is such that the electrons collide at ultra-high speeds against the walls of the device, causing the continuous release of secondary electrons in the medium and leading to a breakdown. However, this is not the critical stage for design implications.

Ionization breakdown is a phenomenon that occurs in gases where the normally low electron density increases in a way similar to an avalanche, turning the isolating gas into conducting plasma; this happens at higher pressures than multipactor. In satellite communications, breakdown analysis must be considered for the components located on Earth and for the ones destined for space operations, since the RF components that are designed to operate in space must be tested frequently on Earth at their highest power and are fully operational during the launching stage for telemetry purposes. This is the reason the analysis is made for low-pressure applications.

Waveguide breakdown analysis follows the next three stages: breakdown threshold determination, circuit and field analysis to determine the maximum voltage or field values and comparison of the experimental worst case with breakdown threshold.

Air ionization is caused because of the electrons' impact against air molecules. These electrons are accelerated by an RF field. If the energy level (provided by the RF field) is enough to cause ionization of neutral molecules, and the free electron total created by ionization exceeds the total losses of electrons due to attachment and recombination, the exponential growth of the electron density generates electron plasma and, eventually, leads to breakdown.

In low pressures, particles have a higher mean free path. Eventually, the mean free path increases until it reaches d (gap distance), where the multipactor effect takes place. By reducing

the atmospheric pressure, there is a lower input power handling capacity until it reaches a minimum operation power; this is called critical pressure [4].

This chapter covers the ionization breakdown in atmospheric air analysis; the equations that describe this consider different processes, such as the ionization, attachment and collision frequencies. Also, the analysis considers as variables the atmospheric pressure and electric field intensity, considering contaminant-free dry air as the propagating medium. Nevertheless, due to the breakdown variability, the design of filters and waveguides is a controversial topic for designers, who consider a wide tolerance range from 0 dB to 3 dB according to minimum breakdown power [4, 5].

Corona breakdown is the process when electron plasma is created due to the ionization of the gas in areas where the electrical fields are high. Electrical fields in filters and waveguides can lead to corona effects at relatively low pressures (from 1 to 100 Torr), which, in atmospheric terms, are reached in the ionosphere (from 80 to 800 km). This phenomenon cannot occur in vacuum conditions, since it is necessary for the presence of a gas to ionize [4].

2. Breakdown power threshold

There are different processes that can generate ions; these are by electronic impact, field effect, photo-ionization and thermos-ionization. For the analysis of filters and waveguides, the most relevant is by electronic impact, being directly proportional to the collision frequency between electrons and molecules. The equation that describes the time evolution of free-electron generation is [4, 6–8]:

$$\frac{\partial n}{\partial t} = \nabla(D\nabla n) - \vec{v} \cdot \nabla n + (v_i - v_a)n - \beta n^2 + P \tag{1}$$

where ν_i and ν_a are the ionization and attachment frequencies, respectively, D is the diffusion coefficient, β is the recombination coefficient and P is the electron production rate by external sources; $\nabla(D\nabla n)$ is the term that defines the diffusion of the electron cloud, from a high-density area to a lower-density area, and is entirely space dependent; and $\vec{v} \cdot \nabla n$ is the convective term that considers the possible movement of the gas.

For the corona effect analysis and from the pre-breakdown stage point of view, the recombination term is discarded, since it is only relevant once the electron density is high enough, which only occurs when the electrical discharge has already begun. Also, the convective term has to be discarded, since a stationary medium is assumed inside the waveguide devices, that is, there is no relevant movement of the gas molecules. Additionally, the diffusion coefficient is considered as space independent, since it is electric field independent [4]. The simplified equation is:

$$\frac{\partial n}{\partial t} = D\nabla^2 n + (v_i - v_a)n \tag{2}$$

Breakdown criteria are based on the fact that the electron density grows very fast once there are more freed electrons than captured. Considering a scenario where there is no diffusion, and

a homogeneous field, due to the similar geometry among the parallel walls of the filter and waveguides. Then, Eq. (2) results in:

$$\frac{\partial n}{\partial t} = (v_i - v_a)n \tag{3}$$

and solving the derivative results in:

$$n(t) = n_0 e^{(v_i - v_a)t}. \tag{4}$$

When $v_i > v_a$, there is an electron avalanche, and the breakdown condition for the continuous waves can be simplified as:

$$\frac{dn}{dt} = 0. \tag{5}$$

As a consequence, the general equation to solve the breakdown threshold stage is:

$$D\nabla^2 n + (v_i - v_a)n = 0. \tag{6}$$

Solving the Laplacian term from Eq. (6), and considering a Cartesian coordinate system, since the devices analysed are rectangular waveguides and filters, the equation leads to:

$$\frac{\partial^2 n}{\partial x^2} + \frac{\partial^2 n}{\partial y^2} + \frac{\partial^2 n}{\partial z^2} + \frac{\nu}{D}n = 0 \tag{7}$$

where $\nu = \nu_i - \nu_a$ is the effective ionization frequency. The rectangular waveguide device must be analysed from the cross-section, so the third term can be discarded, considering only the width and height of the guide.

$$\frac{\partial^2 n}{\partial x^2} + \frac{\partial^2 n}{\partial y^2} + \frac{\nu}{D}n = 0 \tag{8}$$

Establishing the solution as the product of two functions:

$$n(x, y) = X(x)Y(y) \tag{9}$$

Substituting (9) in (8), knowing that the equation components are independent between them, it results in:

$$Y\frac{d^2X}{dx^2} + X\frac{d^2Y}{dy^2} + \frac{\nu}{D}XY = 0 \tag{10}$$

and dividing by (9) we get:

$$\frac{1}{X}\frac{d^2X}{dx^2} + \frac{1}{Y}\frac{d^2Y}{dy^2} + \frac{\nu}{D} = 0. \tag{11}$$

This equation can be solved by proposing exponential solutions. Due to the independency among terms, the first term can be solved proposing a negative constant as a result:

$$\frac{1}{X}\frac{d^2X}{dx^2} = -\sigma$$

$$\frac{d^2X}{dx^2} + \sigma X = 0. \tag{12}$$

An exponential solution for (12) is proposed and derived twice:

$$X(x) = e^{\gamma x} \tag{13}$$

$$X''(x) = \gamma^2 e^{\gamma x}. \tag{14}$$

Substituting (13) and (14) in (12), we get:

$$\gamma^2 e^{\gamma x} + \sigma e^{\gamma x} = 0 \tag{15}$$

It can be determined that:

$$\begin{gathered} \gamma^2 + \sigma = 0 \\ \gamma = \pm\sqrt{-\sigma} \end{gathered} \tag{16}$$

So, the general equation for $X(x)$ is:

$$Ae^{i\sqrt{\sigma}x} + Be^{-i\sqrt{\sigma}x}. \tag{17}$$

By Euler, Eq. (17) can be rewritten as:

$$\begin{gathered} A[\cos\sqrt{\sigma}x + i\sin\sqrt{\sigma}x] + B[\cos\sqrt{\sigma}x - i\sin\sqrt{\sigma}x] \\ (A+B)\cos\sqrt{\sigma}x + (A-B)\sin\sqrt{\sigma}x \\ k_1\cos\sqrt{\sigma}x + k_2\sin\sqrt{\sigma}x. \end{gathered} \tag{18}$$

Considering the next border conditions, since there are no free electrons on the walls of the waveguide:

$$X(0) = 0, \qquad X(a) = 0 \tag{19}$$

where a is the waveguide width distance. Then:

$$\begin{gathered} \mathrm{X}(0) = \mathrm{k}_1 = 0 \\ X(x) = k_2\sin\sqrt{\sigma}x \\ X(a) = k_2\sin\sqrt{\sigma}b = 0 \end{gathered} \tag{20}$$

The only possibility for a non-trivial solution is: $\sin\sqrt{\sigma}b = 0 \Rightarrow \sqrt{\sigma}b = m\pi$; resulting in $\sigma = \left(\frac{m\pi}{a}\right)^2$ where $m = 1, 2, 3, \ldots$. By the same method, the second component of Eq. (11) is: $\sigma_2 = \left(\frac{n\pi}{b}\right)^2$ where $n = 1, 2, 3, 4, \ldots$

This analysis considers the first harmonic. Then, Eq. (8) results in:

$$\left(\frac{\pi}{a}\right)^2 + \left(\frac{\pi}{b}\right)^2 = \frac{\nu}{D} \tag{21}$$

where a and b are the width and height of the rectangular waveguide. MacDonald defined the characteristic diffusion length as [8]:

$$\frac{\nu}{D} = \frac{1}{\Lambda^2} \tag{22}$$

This proves that diffusion processes are entirely dependent on the geometry. If one of the dimensions is much bigger than the other, as in a parallel plates experiment, the characteristic diffusion length is π divided by the squared gap distance. This is valid for rectangular waveguides, due to the fact that they have a constant width and height. For the case of waveguide filters, the shortest height area must be considered for the analysis.

Nevertheless, a more realistic approach implies the presence of non-homogeneous fields, which renders the ionization frequency also non-homogeneous, and, consequently, the free electron density is also affected. To characterize diffusion losses in these situations, the concept of effective diffusion length is described by Ulf Jordan et al. [9].

3. Effective diffusion length

For homogeneous values of D, v_i and v_a, the electron density increasing curve is constant, determined only by the border conditions of the analysed geometry. For non-homogeneous values in space, the free-electron density diffusion curve varies [9].

The inhomogeneity of these parameters occurs because of the inhomogeneity of the microwave electric field, which implies that D and v_a are approximately constant in space, the only inhomogeneous value being $v_i = v_i(x)$.

Ulf Jordan et al. [9] determined that the diffusion length in the presence of non-homogeneous fields also depends on the atmospheric pressure, as shown in Eq. (23). This equation was obtained using computational methods:

$$\frac{1}{\Lambda_{eff}^2} = a^{-2}\sqrt{\pi^4\left(1 + 0.3677\beta\right) + \frac{\pi^2\beta q}{2}} + \left(\frac{\pi}{b}\right)^2 \tag{23}$$

where

$$q = \left(\frac{a}{L_a}\right)^2 + \left(\frac{\pi a}{b}\right)^2$$

a and b are the width and height of the waveguide, respectively, β is a parameter that depends on the used gas (for air $\beta = 5.33$) and the value of L_a is:

$$L_a = \sqrt{\frac{D}{\nu_a}}$$

Consequently, as the pressure increases, the effective diffusion length decreases, and the calculated breakdown thresholds are the same as the ones obtained by using the characteristic diffusion length.

4. Ionization, attachment and diffusion in air

When a microwave field is applied, the energy transfer depends on the field's frequency and the environmental conditions (atmospheric pressure and humidity). An effective electric field is defined as [8]:

$$E_{eff} = \frac{E_{rms}}{\left(1 + \frac{\omega^2}{\nu_c^2}\right)^{\frac{1}{2}}} \tag{24}$$

where E_{rms} is the root mean square electric field, ω is the angular frequency ($2\pi f$) and ν_c is the collision frequency between electrons and molecules. For air, the general equation for the collision frequency is [8]:

$$\nu_c = 5 \times 10^9 p \ \left[\mathrm{s}^{-1}\right] \tag{25}$$

p is the atmospheric pressure in Torr. From Eq. (24) it can be deduced that in high-pressure cases, the effective field is equal to the RMS field, since the collision frequency increases along with the atmospheric pressure.

The diffusion coefficient in air is determined by [8]:

$$D = \frac{10^6}{p}\left[\mathrm{cm}^2\mathrm{s}^{-1}\right]. \tag{26}$$

The ionization frequency can be obtained by [6]:

$$\nu_i = 5.14 \times 10^{11} p \exp\left(-73\alpha^{-0.44}\right)\left[\mathrm{s}^{-1}\right] \tag{27}$$

with

$$\alpha = \frac{E_{rms}}{p\left(1 + \frac{\omega^2}{\nu_c^2}\right)^{\frac{1}{2}}} \equiv \frac{E_{eff}}{p} \tag{28}$$

α is known as the reduced electric field. Eq. (27) is valid in the range of $32 < \alpha < 100$ [4, 6]. The effective field term is very useful, since it relates the properties of the corona in direct current (DC) and alternating current (AC). The effective field produces the same energy transfer as in a DC field, so experimental data can be analysed in DC instead of AC [4, 10, 11]. The attachment frequency is two- and three-body phenomena.

$$\nu_a = \nu_{a2} + \nu_{a3} \tag{29}$$

ν_{a2} is only valid in the range $0 < \alpha < 60$ and is defined as [4, 6]:

$$\nu_{a2} \approx 7.6 \times 10^{-4} p\alpha^2(\alpha + 218)^2 \quad \left[\mathrm{s}^{-1}\right] \tag{30}$$

The three-body attachment is field independent and is obtained as follows [4]:

$$\nu_{a3} = 10^2 p^2 \left[\mathrm{s}^{-1}\right] \tag{31}$$

For electrostatic homogeneous fields:

$$E_b = \frac{V}{d} \tag{32}$$

where d is the structure width and V is the breakdown voltage. Finally, the breakdown power can be obtained by:

$$P = \frac{V^2}{Z} \tag{33}$$

Z is the characteristic impedance of the device. For waveguides and filters, Z is determined by:

$$Z \frac{\sqrt{\mu_0/\varepsilon_0}}{\sqrt{1 - \left(\frac{1}{2fa\sqrt{\mu_0\varepsilon_0}}\right)^2}} \tag{34}$$

μ_0 and ε_0 are the magnetic permeability and the electrical permittivity on vacuum, respectively, and f is the operating frequency.

5. Analytical results' comparison

Commonly, the analytical results obtained by using the characteristic diffusion length are considerably lower than the experimental results at the critical pressure; this minimum power breakdown is known as Paschen minimum. **Figure 3** shows the experimental values obtained by Carlos et al. [4] compared to the analytical results using the characteristic diffusion length, for a low-pass Ku band filter at 12.5 GHz. The experimental and analytical results differ by 16%.

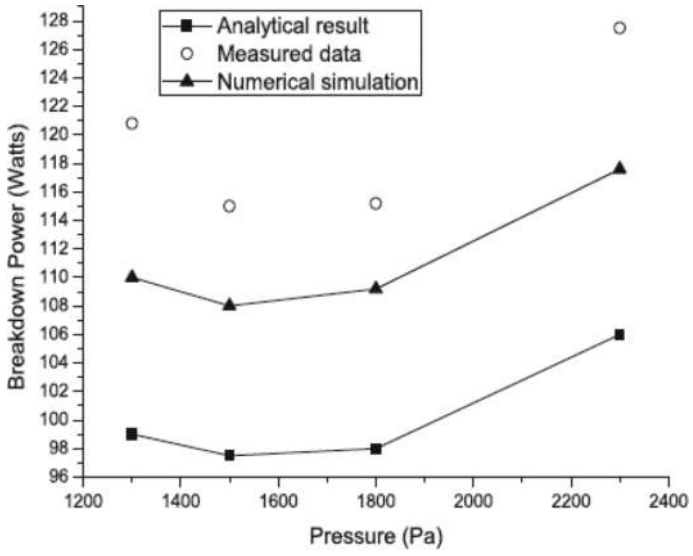

Figure 3. Low-pass Ku band filter operating at 12.5 GHz [4].

The results shown imply that it is necessary to consider the inhomogeneity of the electric fields, not due to geometry but due to the diffusion process that occurs at low pressures [12]. Then, instead of using the characteristic diffusion length, the effective diffusion length is used. **Figure 4** shows the experimental and analytical results using the characteristic diffusion length compared to the analytical results using the effective diffusion length for the same low-pass filter.

Figure 5 shows another result comparison but for a corrugated waveguide filter operating at 12.2 GHz.

Figures 4 and **5** show a slight increase in breakdown power, proving that the effective diffusion length from Eq. (23) is a more suitable equation for the cases of waveguide devices where the field inhomogeneity is greater.

These results can be explained because microwave breakdown in an RF device is manifested by an avalanche-like growth in time of the free-electron density in the gas filling the device. The difference between these power threshold results resides not only in their operating frequency but in their geometries and the number of irregularities the filter contains. A bigger amount of irregularities, or irises (steps that help in the filtering process), contributes to generating more inhomogeneity on the electric field.

Figure 6 shows the transversal configuration and measures of each filter [4].

For the analysis of each filter, the minimum length located in the middle is considered.

The filter operating at 12.5 GHz is affected by the electric field inhomogeneity more than the other because of its high number of irises. Predicting mathematically the breakdown

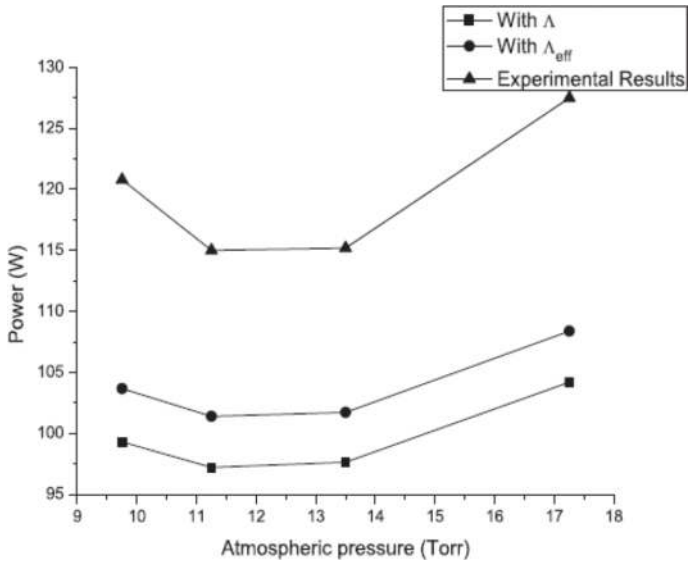

Figure 4. Experimental and analytical results using Λ and Λ_{eff} for a Ku band filter operating at 12.5 GHz.

threshold of a device with high amount of irregularities, such as **Figure 6** (b), requires modifications to the equations, more specifically, the use of an effective field-dependent collision frequency equation. The large number of irises generates a much higher space charge density than for a conventional obstruction-free waveguide. Further analysis of space charge density and the correct equations for these cases are considered in Section 6.

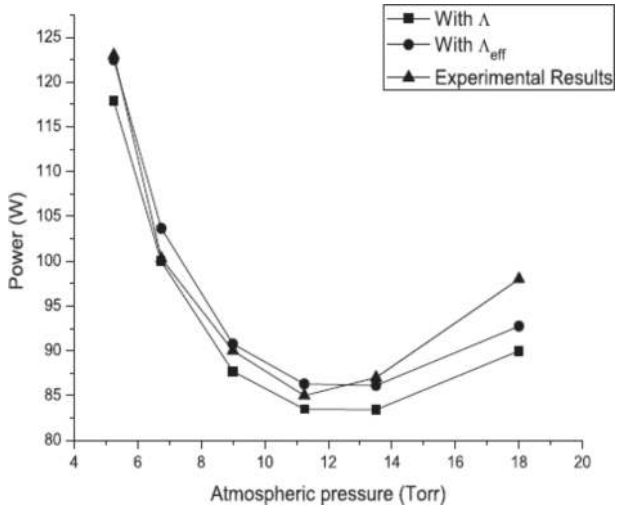

Figure 5. Experimental and analytical results using Λ and Λ_{eff} for a Ku band filter operating at 12.2 GHz.

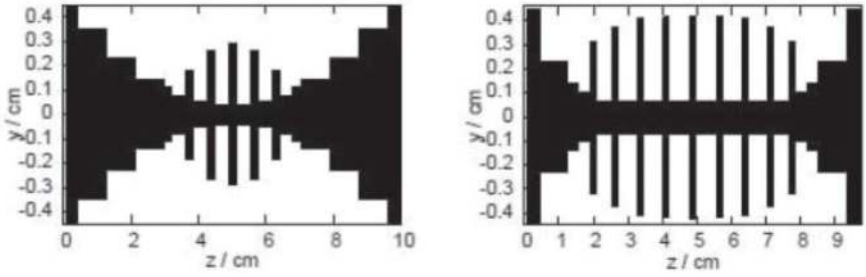

Figure 6. Transversal configuration of waveguide filters. (a) Operating at 12.2 GHz. (b) Operating at 12.5 GHz [4].

Analysed filter		Minimum breakdown power [W]	Data rate [Gb/s]
12.2 GHz	Λ	83.5	4175
	Λ_{eff}	86.1	4305
12.5 GHz	Λ	97.2	4860
	Λ_{eff}	101.4	5070

Table 1. Calculated bit rate from power obtained by characteristic diffusion length and effective diffusion length for two different Ku band filters.

According to Witting [13], the transmission capacity of a communication network in terms of the number of users, power and data rate is:

$$\frac{R_B \cdot N}{P} \leq 20 \times 10^{18} \left[\mathrm{W}^{-1}\mathrm{s}^{-1}\right] \tag{35}$$

where R_B is the data rate in bits/s, N is the number of users and P is the power in watts. **Table 1** shows the difference of bit rate obtained with the power from characteristic diffusion length calculation and the one from effective diffusion length calculation for the two different Ku band filters.

By using (35), the resulting increase on the bit rate of the filters, when using the effective diffusion length, is of 4.3% in the case of the 12.5 GHz low-pass filter and of 3.1% for the 12.2 GHz low-pass filter. Therefore, a small raise in the power, even of 3 or 4 W, is heavily reflected on the data rate and an increase of almost 200 Gbps is achieved.

6. Space charge density effects

The microwave devices' designers use the analytical solution of the corona discharge to determine if the operating power is within the established margins. As shown previously, the experimental results differ considerably from the analytical when the characteristic diffusion length is considered. It has been proved by some authors [2, 9, 12, 14] that the criteria used until now for the design of waveguide filters can be improved if the effective diffusion length is used instead of the characteristic diffusion length.

http://dx.doi.org/10.5772/intechopen.76973

The two main processes responsible for the electron losses during the breakdown stages are the diffusion from high-density regions towards lower-density regions and the attachment by neutral molecules, forming essentially negatively charged unmovable ions. For sufficiently enough electron density, at breakdown threshold, the region saturates and the electric field propagation is affected by its reflection or absorption in the device walls.

The most important negative ions present in air are O_2^- and O^- and the most important positive ions formed during electrical breakdowns at atmospheric pressure are N_2^+, N_4^+ and O_2^+. There have not been negative ions detected for nitrogen experimentally [15].

The avalanche evolution can be affected by any agent that alters the space charge electronic density. **Figure 7** shows the electric field E_r around the avalanche and the resulting modification of the applied field E_0. The space charge at the head of the avalanche is assumed as concentrated within a spherical volume, with the negative charge ahead because of the higher electron mobility. The field is enhanced in front of the head of the avalanche with field lines from the

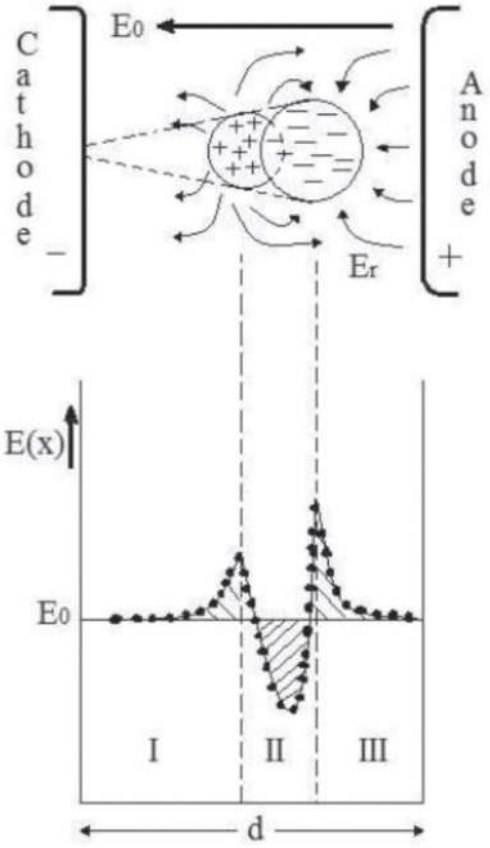

Figure 7. Schematic representation of electric field distortion in a gap caused by space charge of an electron avalanche [16].

anode terminating at the head, the region III. Further back in the avalanche, the field between the electrons and the ions left behind reduced the applied field (E_0), the region II. Still, further back, the field between the cathode and the positive ions is enhanced again, the region I [16].

The resultant field strength in front of the avalanche is thus ($E_0 + E_r$), whereas in the positive ion region just behind the head the field is reduced to a value ($E_0 - E_r$).

According to the results exhibited in **Figures 4** and **5**, where the analytical values of the breakdown power are lower than the experimental ones, this is an indication that the avalanche is mainly affected by the presence of positively charged ions instead of the negatively charged ions. The radial field produced by positive ions immediately behind the head of the avalanche can be calculated using the expression from [16]:

$$E_r = 5.3 \cdot 10^{-7} \frac{\alpha e^{\alpha_T x}}{\left(\frac{x}{p}\right)^{\frac{1}{2}}} \left[\frac{\text{Volts}}{\text{cm}}\right] \tag{36}$$

where x is the distance in cm in which the avalanche has progressed, p is the gas pressure in Torr and α is the Townsend first coefficient of ionization, denoted by:

$$\alpha_T x = 17.7 + \ln x \tag{37}$$

The Townsend first ionization coefficient indicates the number of ions generated by the electron collision by length unity. **Figure 8** shows the behaviour of E_r and E_0 as a function of the pressure for different values of x, $x = a = 0.25$ cm, as this is the maximum height of the analysed Ku band filter.

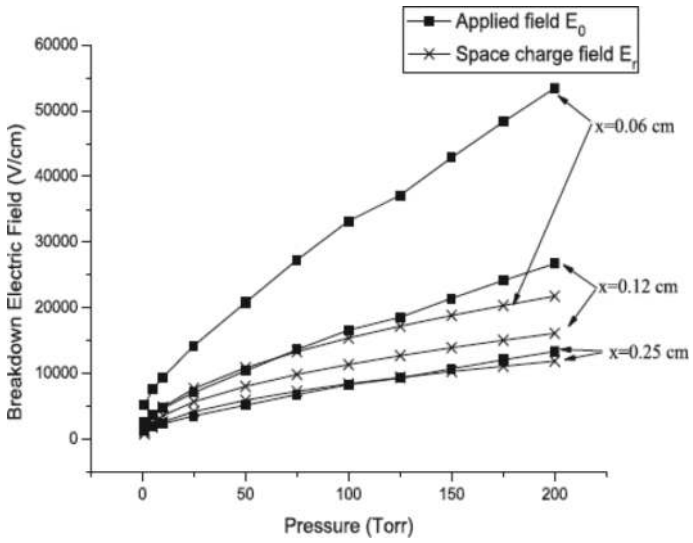

Figure 8. Applied electric breakdown E_0 versus space charge electric field E_r for different values of x.

It can be appreciated that the influence of the positive ionic space charge field is greater as a function of the development in the space of the avalanche.

For a more correct approach of the analytical results, Woo et al. [6] propose the collision frequency equation dependent on the reduced electric field as:

$$\nu_c = 5 \times 10^9 p \left[\frac{\alpha}{\alpha + 8}\right]^{1/2}. \tag{38}$$

Figures 9 and **10** show the results of using this energy-dependent collision frequency equation and the effective diffusion length.

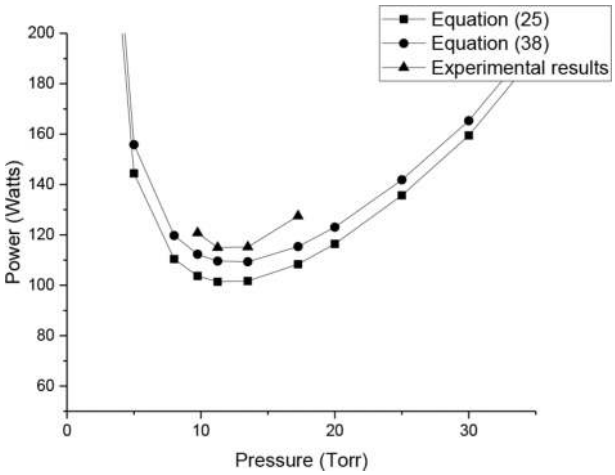

Figure 9. Breakdown power of a Ku band filter operating at 12.5 GHz using different collision frequency values.

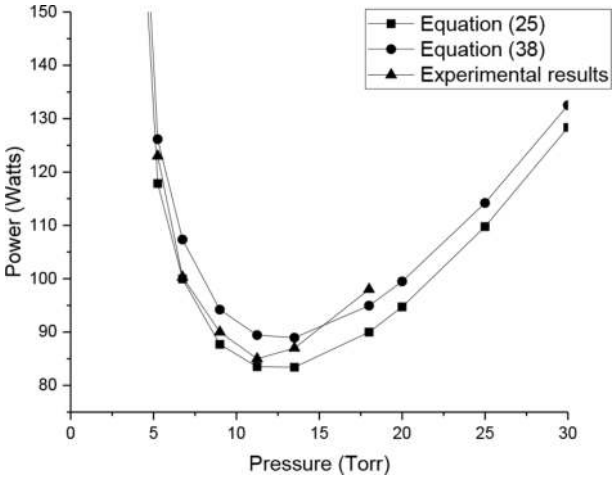

Figure 10. Breakdown power of a Ku band filter operating at 12.2 GHz using different collision frequency values.

It is shown that considering the diffusion length and the electric field-dependent collision frequency altogether, the results are far more similar to the experimental results, proving this to be an important approach towards the experimental results.

As minimal as these increases result, **Table 1** shows the importance of power, and the regulations for the design of these devices can be increased in terms of input power tolerance.

7. Plasmonic waveguide filters for increased data rate transmission

As the actual waveguide devices reach the technological limit, in terms of their data rate, it is necessary to develop new alternatives to overcome the continuously increasing demand of services [12]. By using encoding techniques, it is possible to send up to 16 bits of information per each Hertz sent [17]; the current Ku band analysed devices operate generally around 12.2 GHz, so the data rate is only of 195.2 Gbps. Much higher frequencies, such as those provided by optical communication, of about 350 THz, show a much promising environment, delivering up to 5600 Tbps.

Optical wireless communications demand different multiplexing and de-multiplexing techniques than traditional RF communication. For this, some proposals include a wavelength divisor multiplexer (WDM), this can be a polymer substrate mode for photonic interconnections and is used even for satellite communications [18]. This helps in a way that incoming signals are directly coupled with the system chip, leaving out any optical-electrical and electrical-optical conversions. This is a partial solution since the system needs power and wavelength management; for this, digital grating processors (DGPs) are implemented. There are many advantages that these photonic interconnections provide, among them are introducing a planar platform for space-saving purposes, efficiency against any external perturbation, low propagation losses, compatibility with other surface mount technologies and low cost. Nevertheless, DGPs are components that demand energy from the system to operate and generate interruptions in the transmission due to electronic processing. Other components can be responsible for the filtering of signals; as seen by Calva et al. [2], a plasmonic waveguide filter is a viable option.

Since the interconnection is very important, as the planar configuration of the devices, plasmonic waveguide filter proves a viable solution due to their capability of transfer information operating at different frequencies at the same time. Surface plasmons' inherent properties permit the signal to travel at the speed of light and also transport electrical and optical signals simultaneously [19]. The disadvantage of using these devices is that electrical breakdown due to ionization phenomena can occur.

These particular devices' operating principle is based on the light capability to penetrate some materials; for metals this can be up to 30 nm deep, helping in the generation of surface plasmons, which are oscillating free electrons in a coherent state that generate at the interface between any two materials. In some cases, incident light couples with the surface plasmon to generate self-sustaining propagating electromagnetic waves; these are known as surface plasmon polaritons (SPPs) [19]. A plasmonic waveguide filter example is shown in **Figure 11**; this is based on a metal–insulator–metal (MIM) structure [20].

http://dx.doi.org/10.5772/intechopen.76973

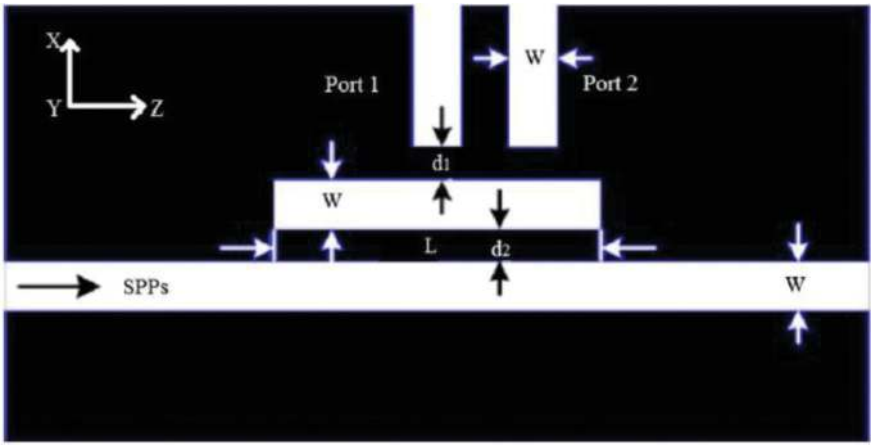

Figure 11. Two-channel plasmonic waveguide filter structure.

The configuration of these filters is formed by stacking nanometric waveguides of the same gap length. Multiple resonance modes are formed inside the devices; only the first and second mode can traverse through the next waveguides, the one in the middle of **Figure 11** and the port 1 and 2 vertical waveguides. The SPPs travel through the principal plasmonic waveguide; resonance happens if the SPPs are enclosed in the middle cavity. This mid-section is very important, since its size is responsible for the filtering effect; modifications of its length alter the delivered wavelength through ports 1 and 2. A wide range of wavelengths can be covered by using these filters, from 500 to 10,000 nm. However, some optimal configurations have been suggested; for distances of L=280, 320, 350, 360, and 390 nm, the transmitted resultant wavelengths are λ=575, 850, 1060, 1310, and 1550 nm, respectively [2]. As mentioned before, it is imperative to consider the field skin deep so that light can travel through the metal of these waveguide structures; d_1 and d_2 distances must be smaller than 30 nm in the case of silver [21]. The field skin deep distance describes the length of a given material, silver in this case, that an electromagnetic signal can penetrate, this distance depends on the signal frequency and the material properties. So, in this case, the distances are 10 and 15 nm, respectively, with a gap distance for all the waveguides of $W = 50$ nm. These filters have very good transmission spectra and can easily operate in wavelengths from 575 to 1500 nm, optimal for using them for an optical communication scheme.

The analysis of electromagnetic waves through a surface already excited contemplates that the electrons are in a non-equilibrium state and that they are generated because of light absorption, not only due to collisions. The absorption can be linear or multiple, resulting in many non-equilibrium electrons; then, considering the diffusion effect, electron–electron collisions occur and there is an energy exchange between the photon-excited electrons and the non-equilibrium electrons. The evolution in time of the free-electron density generated by excited photons and electron–electron collisions is [22]:

$$\frac{\partial n}{\partial t} = D\nabla^2 n + \frac{(1-R)\alpha_1 I}{\hbar\omega} + \frac{(1-R)^2\alpha_2 I^2}{2\hbar\omega} - \frac{n}{\langle\tau_{ee}\rangle} \tag{39}$$

where D is the electronic diffusion coefficient, $\langle\tau_{ee}\rangle$ is the time between the electron–electron collisions, I is the irradiance of light in watts per square meter, R is the reflection coefficient, α_1 is the linear photonic absorption coefficient and α_2 is the two-photon absorption coefficient.

According to Bhushan et al. [23], there is no two-photon absorption for the cases where the plasmon has an angular momentum of $l > 1$ kgm^2/s. $l = 1$ corresponds to the bipolar resonance of the plasmon, which is the one that occurs in these types of filters [20]. Then, Eq. (39) is reduced to the following:

$$\frac{1}{\Lambda_{eff}} = \left(\frac{(1-R)\alpha_1 I}{\hbar\omega} - \frac{n}{\langle\tau_{ee}\rangle}\right)/nD \tag{40}$$

Substituting $\frac{1}{\langle\tau_{ee}\rangle} = \nu_c$:

$$\frac{1}{\Lambda_{eff}} = \frac{(1-R)\alpha_1 I}{\hbar\omega nD} - \frac{\nu_c}{D} \tag{41}$$

The lineal photonic absorption is obtained using the following [24]:

$$\alpha_1 = 4\pi\bar{k}/\lambda \ \left[\text{cm}^{-1}\right], \tag{42}$$

where $\bar{k}$ is the extinction coefficient. **Table 2** shows the experimentally obtained values in [24] for the extinction coefficients at a specific wavelength and the corresponding absorption coefficients.

The electron density in the electrical breakdown threshold is $n = 1.1 \times 10^{15}\text{cm}^{-3}$ [25]. The reflection coefficient of silver is $R = 0.95$. The $\hbar\omega$ term is the energy of a photon, where $\hbar$ is the Planck's constant divided by 2π:

$$\hbar\omega = \frac{h2\pi f}{2\pi} = hf = 6.62 \times 10^{-34} f[\text{J}] \tag{43}$$

Using these equations and the effective diffusion length, as discussed before, in (39) the power breakdown threshold of a plasmonic waveguide filter can be obtained. **Figure 12** shows the power breakdown threshold of a plasmonic waveguide filter at different wavelengths.

Wavelength [**nm**]	**Extinction coefficient** $\bar{k}$	**Absorption coefficient** $\left[\text{cm}^{-1}\right]$
575	3.45	7.54E + 05
850	5.70	8.43E + 05
1060	7.33	8.69E + 05
1310	9.10	8.73E + 05
1550	10.60	8.59E + 05

Table 2. Experimental values for the extinction and linear photonic absorption coefficients.

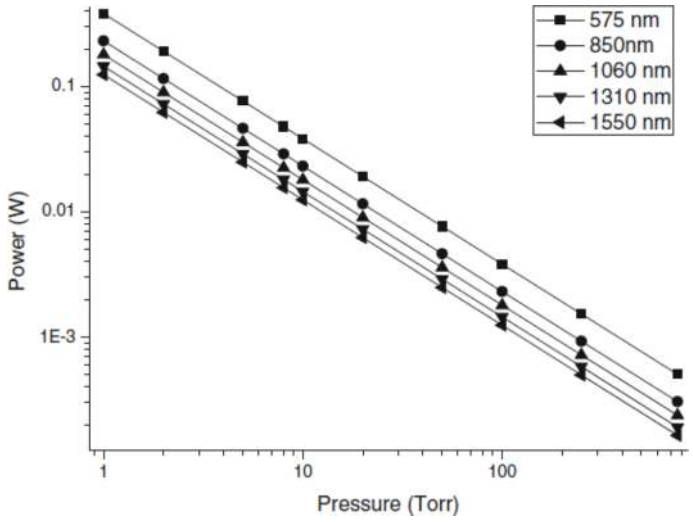

Figure 12. Power breakdown threshold of a two-channel plasmonic waveguide filter at different wavelengths.

These extremely low power values are not a problem in the data transmission, according to Radek Kvicala et al. [26]; the optical communication systems are capable of receiving very low optical powers of about $P = 4 \times 10^{-14}$ Watts.

8. Conclusions

The suggested modifications to the waveguide devices breakdown threshold analysis change the operating power in terms of the continuously increasing bandwidths and component integration. Increasing power handling in these devices by just a few watts have a considerable effect in the data rate, increasing its value, whereas avoiding the risk of breakdown to occur.

Waveguide designers use the free electrons in the time equation to obtain the lowest possible breakdown thresholds, which implies that homogeneous electric fields as a function of the geometry are considered. However, the presence of space charge inside the devices causes inhomogeneities in the electric field; therefore, it is important to determine the device structure for a correct analysis. When analysing a waveguide filter, the substructures inside it that generate the filtering effect, highly non-homogeneous areas are located. In these cases, the use of the effective diffusion length, along with the collision frequency equation that highly depends on the electric field, must be imperative for a correct approximation of the real values.

Plasmonic waveguide filters are a good proposal for the implementation of higher-frequency technologies. For wavelengths from 575 to 1500 nm, the power breakdown threshold is located between 0.1 and 0.4 Watts at 1 Torr atmospheric pressure. These power thresholds are

sufficient for the electronic processing required in an optical environment, since optical systems are capable of fully operating while receiving very low power, $P = 4 \times 10^{-14}\ W$.

Author details

Isaac Medina[1,2]* and Primo-Alberto Calva[1,2]

*Address all correspondence to: ismesa@gmail.com

1 Centro de Desarrollo Aeroespacial del Instituto Politécnico Nacional, Delegación Cuauhtémoc, México, Ciudad de México

2 Instituto Politécnico Nacional, Colonia Barrio la Laguna Ticomán, Delegación Gustavo A. Madero, México, Ciudad de México

References

[1] Elbert BR. Introduction to Satellite Communication. London: Artech House; 2008

[2] Calva PA, Medina I. Power Breakdown Threshold of a Plasmonic Waveguide Filter. Plasmonics, Springer US; January 2014

[3] Marcuvitz N. Waveguide Handbook. London, United Kingdom: Peter Peregrinus Ltd.; 1985

[4] Vicente Quiles CP. Passive intermodulation and corona discharge for microwave structures in communications satellites. Dissertation PhD Thesis, Germany: Technischen Universitat Darmstadt zur Erlangung der Wurde; 2005

[5] Ming Y. Power- handling capability for RF filters. IEEE Microwave Magazine. October 2007:88-97

[6] Woo W, DeGroot J. Microwave absorption and plasma heating due to microwave breakdown in the atmosphere. IEEE Physical Fluids. 1984;**27**(2):475-487

[7] MacDonald AD. Microwave Breakdown in Gases. New Jersey, United States: John Wiley & Sons; 1966

[8] MacDonald AD, Gaskell DU, Gitterman HN. Microwave breakdown in air, oxygen and nitrogen. Physical Review. June 1963;**130**:1841-1850

[9] Jordan U, Anderson D, et al. On the effective diffusion length for microwave breakdown. IEEE Transactions on Plasma Science. 2006;**34**(2):421-430

[10] Scharfman WE, Morita T. Voltage Breakdown of Antennas at High Altitude. Proceedings of the IRE, November 1960, pp. 1881-1887

[11] Ali AW. Intense and Short Pulse Electric Field (DC and Microwave) Air Breakdown Parameters. Washington, DC: Naval Research Laboratory; August 29, 1986. pp. 1-34

[12] Calva PA, Medina I. New solutions of the corona discharge equation for applications in waveguide filters in SAT-COM. IEEE Transactions on Plasma Science. April, 2013;**41**(4)

[13] Witting M. Satellite onboard processing for multimedia applications. IEEE Communications Magazine. June 2000;**38**(6):134-140

[14] Jordan U, Anderson D, Semenov V, Puech J. Discussion on the effective diffusion length for microwave breakdown. Institute of Applied Physics RAS. pp. 1-2

[15] Badaloni S, Gallimberti I. Basic data of air discharges: UPee - 72/05 Report, June 1972

[16] Kuffel E, Zaengl WS. High Voltage Engineering. London UK: Newnes; 2000

[17] International Telecommunications Union. Handbook on Satellite Communications. New York: Wiley; 2002

[18] Liu J, Gu L, Chen R, Craig D. WDM polymer substrate mode photonic interconnects for satellite communications. Photonics packaging and integration IV, Proceedings of SPIE, vol. 5358 (SPIE, Bellingham, WA); 2004

[19] Novotny L, Hecht B. Principles of Nano-Optics. Cambridge: Cambridge University Press; 2006

[20] Wen K, Yan L, Pan W, Luo B, Guo Z, Guo Y. Wavelength demultiplexing structure based on a plasmonic metal-insulator-metal waveguide. Journal of Optics, IOP Publishing. 2012; **14**(7):1-5

[21] Dionne JA, Sweatlock LA, Atwater HA. Plasmon slot waveguides: Towards chip-scale propagation with subwavelength-scale localization. Physical Review B. 2006;**73**(035407)

[22] Martsinovsky GA, et al. The role of plasmon-polaritons and waveguide modes in surface modification of semiconductors by ultrashort laser pulses, Fundamentals of laser assisted micro- and nanotechnologies. Proceedings of SPIE, Vol. 6985; 2008

[23] Bhushan B, Kundu T, Singh BP. Two photon absorption spectrum of silver nanoparticles. Optic Communication; **285**:5420-5424

[24] Palik ED. Handbook of Optical Constants of Solids. New York: Academic; 1991

[25] Unnikrishnan VK, Kamlesh A, et al. Measurements of plasma temperature and electron temperature in laser-induced copper plasma by time-resolved spectroscopy of neutral atom and ion emissions. Pramana-Journal of Physics. 2010;**74**

[26] Kvicala R, Hampl M, P Kucera. Satellite terrestrial (Earth) station optical communication. Northern Optics, Bergen, IEEE; 2006. pp. 83-85